PCCP

RSC Publishing

COMMUNICATION

View Article Online
View Journal | View Issue

Roughening of Pt nanoparticles induced by surface-oxide formation

Cite this: *Phys. Chem. Chem. Phys.*, 2013, **15**, 2268

Received 28th November 2012,
Accepted 11th December 2012

DOI: 10.1039/c2cp44252c

www.rsc.org/pccp

Tianwei Zhu,[ab] Emiel J. M. Hensen,[a] Rutger A. van Santen,[a] Na Tian,[b] Shi-Gang Sun,[b] Payam Kaghazchi*[c] and Timo Jacob[c]

Using density functional theory (DFT) and thermodynamic considerations we studied the equilibrium shape of Pt nanoparticles (NPs) under electrochemical conditions. We found that at very high oxygen coverage, obtained at high electrode potentials, the experimentally-observed tetrahexahedral (THH) NPs consist of high-index (520) faces. Since high-index surfaces often show higher (electro-)chemical activity in comparison to their close-packed counterparts, the THH NPs can be promising candidates for various (electro-)catalytic applications.

High-surface area nanoparticles (NPs) are widely used as industrial catalysts for many chemical reactions. Smaller NPs are often more active toward chemical reactions due to their larger surface area to volume ratio and higher density of low-coordinated atoms at edges and corners.[1–3] The shape of NPs also plays a key role in the performance of catalysts:[1] the NPs with atomically-open (high-index) surfaces are often more active than those with close-packed (low-index) surfaces.[4] The metal nanoparticles enclosed by high-index faces are, however, unfavorable due to their high formation energy. Hence, it is desirable to find a method to synthesize atomically-rough NPs that remain stable during (electro-)catalytic reactions.

Pt NPs are of great interest for the petrochemical industry,[5,6] fuel-cell technology,[7] and automobile exhaust purification.[4] The Pt NPs, synthesized in the past, are usually enclosed by close-packed faces.[8] However, high-index Pt surfaces possess much higher catalytic reactivity for (electro-)catalytic reactions: *e.g.* Pt(210) for electro-reduction of CO_2[9] and electro-oxidation of formic acid;[10] Pt(410) for catalytic decomposition of NO.[11] Recently, we prepared Pt NPs with a tetrahexahedral (THH) shape from Pt nanospheres under electrochemical conditions using a square-wave potential.[8] Transmission electron microscopy (TEM) images have shown that they consist of 24 high-index faces. Furthermore, the THH Pt NPs were found to be stable thermally and chemically and have greater activity toward electro-oxidation of small organic fuels such as formic acid and ethanol in comparison to those consisting of low-index (*i.e.* Pt(111) and Pt(100)) facets.[8]

Here, by using DFT and thermodynamics consideration we study the structure of Pt NPs under electrochemical conditions. We show that the experimentally-observed THH NPs consist of (520) faces, which become more stable than low-index faces at high potentials (≥ 1.24 V) due to O-induced reconstruction and surface-oxide formation.

We first summarize the TEM results reported by Tian *et al.*:[8] Pt NPs were synthesised by electro-deposition of polycrystalline Pt nanospheres on glassy carbon in a solution of 2 mM K_2PtCl_6 + 0.5 M H_2SO_4 followed by treatment with square-wave potential (10 Hz, upper potential 1.20 V, lower potential between −0.10 and −0.20 V) in a solution of 0.1 M H_2SO_4 and 30 mM ascorbic acid for 10 to 60 min. TEM images indicate that most of the NPs obtained by this method have the perfect THH shape as can be seen in Fig. 1(a). This shape can be bound by (210) or its vicinal surfaces (*e.g.* (520) and (730)). Comparing the measured and calculated angles between facets demonstrates that (520) or (730) orientations are dominant. In addition, some of the synthesized Pt NPs show an irregular THH shape (see Fig. 1(b)), which based on our analysis can be enclosed by (100) in addition to (520) or (730) faces.

The equilibrium shape of NPs is governed by the minimization of the overall Gibbs free energy, which is mainly the sum of surface, edge, corner, and strain contributions. For large particles (usually >3–5 nm) the formation energy is dominated by the surface contributions only and the equilibrium shape can then be obtained by:

$$\min \sum_i \gamma_i A_i. \quad (1)$$

In this so-called Wulff theorem[12] γ_i and A_i are the surface free energy and the area of the ith face of the particle, respectively.

Previous studies have used the *ab initio* atomistic thermodynamics approach[13–16] to calculate the stability of different

[a] *Department of Chemical Engineering and Chemistry, Eindhoven University of Technology, The Netherlands*
[b] *State Key Laboratory of Physical Chemistry of Solid Surfaces, Department of Chemistry, College of Chemistry and Chemical Engineering, Xiamen University, Xiamen, 361005, China*
[c] *Institut für Elektrochemie, Universität Ulm, Albert-Einstein-Allee 47, D-89081 Ulm, Germany. E-mail: payam.kaghazchi@uni-ulm.de*

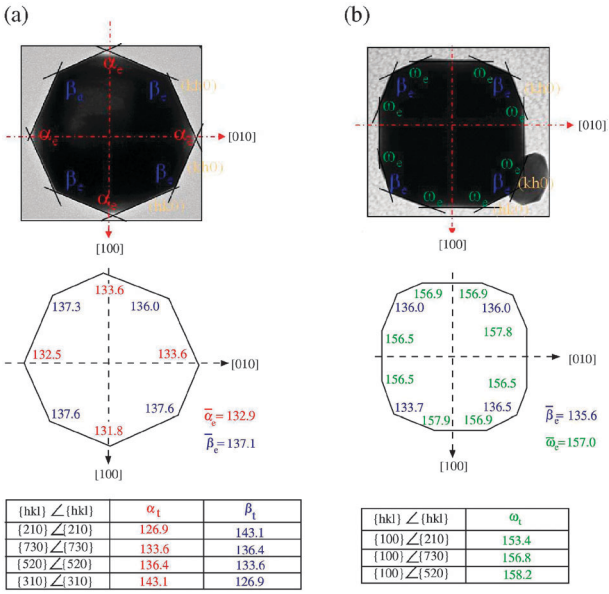

{hkl} ∠ {hkl}	α_t	β_t
{210} ∠ {210}	126.9	143.1
{730} ∠ {730}	133.6	136.4
{520} ∠ {520}	136.4	133.6
{310} ∠ {310}	143.1	126.9

{hkl} ∠ {hkl}	ω_t
{100} ∠ {210}	153.4
{100} ∠ {730}	156.8
{100} ∠ {520}	158.2

Fig. 1 TEM image of the (a) perfect and (b) irregular THH Pt NP and their measured interfacial angles [given in deg.] α_e, β_e, ω_e and their corresponding average values $\bar{\alpha}_e$, $\bar{\beta}_e$, $\bar{\omega}_e$. Theoretical values of the interfacial angles α_t, β_t, ω_t that have been obtained by geometrical considerations are listed in the tables.

facets and obtain the equilibrium shape of metal NPs (using eqn (1)) such as Rh and Pd in contact with an oxygen atmosphere.[17] In the present work, the surface free energies of different Pt facets are evaluated by the extended *ab initio* atomistic thermodynamics approach.[18,19] This approach allows calculating the stability of electrode–electrolyte interfaces (under electrochemical conditions), which depends on temperature T as well as the activity a_i and electrostatic potential ϕ_i of the reservoir containing the ith-species (here Pt and O):

$$\gamma(T,\{a_i\},\{\phi_i\}) = \frac{1}{A}\left[G^{\text{interf}}(T,\{a_i\}) - \sum_i N_i\mu_i(T,\{a_i\},\{\phi_i\})\right]. \quad (2)$$

Here, A is the surface area, G^{interf} is the Gibbs energy of the interface, and N_i is the number of atoms of the ith-species, whose reservoir is characterised by the chemical potential $\mu_i(T,\{a_i\},\{\phi_i\})$. For a Pt electrode in contact with an aqueous electrolyte we assume that every oxygen that desorbs from the interface produces water by reacting with two electrons from the working electrode at the potential ϕ_{we} and two protons from the electrolyte.

$$H_2O \rightleftharpoons \frac{1}{2}O_2 + 2H^+ + 2e_{\text{we}}{}^-. \quad (3)$$

The presence of a reversible counter electrode (*e.g.* reversible hydrogen electrode) at the potential ϕ_{re} would compensate each proton generated during the splitting of water to produce O^{2-} by an immediate hydrogen evolution reaction:

$$2H^+ + 2e_{\text{re}}{}^- \rightleftharpoons H_2. \quad (4)$$

The chemical potential of O for reactions (3) and (4) is

$$\begin{aligned}\mu_O &= \mu_{H_2O} - 2\left[\frac{1}{2}\mu_{H_2} + e\phi_{\text{re}}\right] + 2e\phi_{\text{we}} \\ &= \mu_{H_2O} - \mu_{H_2} + 2e\Delta\phi.\end{aligned} \quad (5)$$

Here, $\Delta\phi$ is the potential difference between ϕ_{we} and ϕ_{re}. The chemical potentials of water and hydrogen can be written as

$$\begin{aligned}\mu_{H_2O} &= \bar{\mu}_{H_2O}(T,a^0) + k_B T \ln\left(\frac{a_{H_2O}}{a^0}\right) \\ \mu_{H_2} &= \bar{\mu}_{H_2}(T,p^0) + k_B T \ln\left(\frac{p_{H_2}}{p^0}\right)\end{aligned} \quad (6)$$

Combining eqn (5) and (6) we have

$$\begin{aligned}\mu_O &= \frac{1}{2}E_{O_2}^{\text{tot}} + \Delta G_{O_2}^{H_2O} + \bar{\mu}_{H_2O}(T,a^0) + k_B T \ln\left(\frac{a_{H_2O}}{a^0}\right) \\ &\quad - \bar{\mu}_{H_2}(T,p^0) - k_B T \ln\left(\frac{p_{H_2}}{p^0_{H_2}}\right) + 2e\Delta\phi,\end{aligned} \quad (7)$$

where $\Delta G_{O_2}^{H_2O}$ is the Gibbs energy required to form $1/2O_2$ out of liquid water. In the present work we use experimental values for $\Delta G_{O_2}^{H_2O}$ (2.46 eV[20]) as well as the standard chemical potentials $\bar{\mu}_{H_2O}$ and $\bar{\mu}_{H_2}$. Finally, by combining eqn (2) and (7) we can evaluate the stability of O/Pt surfaces *versus* $\Delta\phi$ using

$$\begin{aligned}\gamma(T,p,\Delta\phi) \approx \frac{1}{A}\Big[&E_{\text{tot}}^{\text{interf}} - N_{Pt}E_{\text{tot}}^{Pt} - N_O \\ &\times\left(\frac{1}{2}E_{O_2}^{\text{tot}} + \Delta G_{O_2}^{H_2O} + \bar{\mu}_{H_2O}(T,a^0) + k_B T \ln\left(\frac{a_{H_2O}}{a^0}\right)\right. \\ &\left. - \bar{\mu}_{H_2}(T,p^0) - k_B T \ln\left(\frac{p_{H_2}}{p_{H_2}^0}\right) + 2e\Delta\phi\right)\Big].\end{aligned} \quad (8)$$

Here, the difference in the Gibbs energies of the interface (slab) and the bulk phases has been replaced by their corresponding total energies, which then can be evaluated using DFT.

To study the shape of Pt NPs we took into account the following surfaces in the Wulff construction: (i) the low-index (111), (100) and (110) surfaces that are usually expected to dominate the surface of Pt NPs in contact with an oxygen atmosphere under UHV conditions[21] and (ii) the (210), (520) and (730) surfaces that we propose as possible faces of the THH Pt NPs.

We have shown previously that adsorbate-induced restructuring requires strongly interacting adsorbates.[22] As the binding energy of O is roughly 1.2–1.4 eV stronger[23] than that of water or OH on Pt, the latter adsorbates will not cause the particle shapes as discussed in our work to form. Moreover, in recent studies we found that co-adsorbed water and/or OH has a minor effect on the oxygen binding energy.[24] Therefore, in the present work we concentrate on oxygen only. As surface oxygen is expected to induce the formation of THH Pt NPs, we performed DFT calculations[25] on the adsorption of oxygen over the Pt surfaces. To permit surface reconstruction to occur we have used relatively large unit cells in our calculations: (3 × 3) unit cells for the (111), (100), and (110) surfaces and (2 × 1) unit cells for the (210),

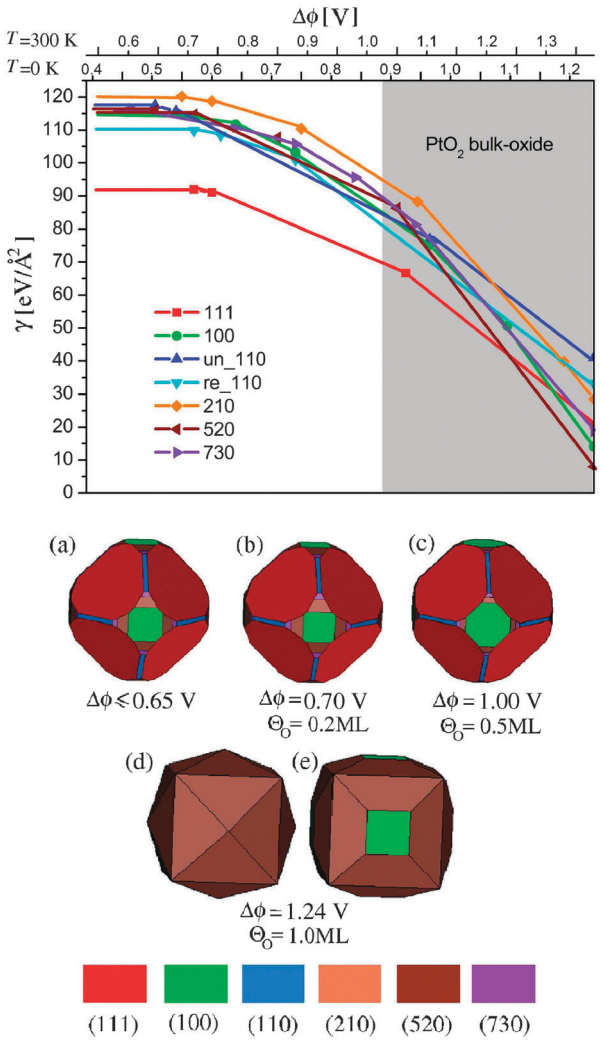

Fig. 2 Electrochemical phase diagram for the electro-oxidation of Pt surfaces showing the surface stability γ as a function of the electrode potential $\Delta\phi$ at zero and room temperature for a_{H_2O} = 1 and p_{H_2} = 1 atm (see eqn (8)). The phase diagram shows the conditions under which the different phases are thermodynamically stable. The region at which the bulk-oxide (PtO_2) is stable is in grey. The equilibrium shape of Pt nanoparticles at selected low (a and b), medium (c) and high (d and e) values of $\Delta\phi$ are presented at the bottom of the phase diagram.

(520) and (730) surfaces. In addition, for (110) we also considered possible missing-row reconstruction of $1 \times n$ (n = 1,2,3,4).

Fig. 2 is the resulting phase diagram showing surface free energy *versus* $\Delta\phi$ for the electro-oxidation of Pt surfaces and NPs. The overall surface energy has been minimized with respect to the shape of NPs (see eqn (1)), while the free energy of each surface with respect to the O coverage, *i.e.* N_O/A (see eqn (8)). As mentioned above, here we assume that each oxygen comes from the water splitting reaction induced by the applied electrode potential, which also tunes the amount of oxygen that adsorbs on the surface.

The phase diagram shows that for each Pt surface below a critical $\Delta\phi$ where no oxygen is adsorbed on the surface γ remains constant (horizontal lines). Above this critical electrode potential, oxygen atoms start binding to the surface (non-horizontal lines), while the coverage of O on the surface increases gradually with $\Delta\phi$ (the higher the coverage, the steeper the slope).

Using the calculated γ for different surfaces and coverages, we then constructed the Wulff shapes of Pt satisfying eqn (1) as a function of $\Delta\phi$. The coverage of O on the NP (Θ_O) for different $\Delta\phi$ that is shown in Fig. 2 is the weighted average value given in ML, where 1 ML corresponds to the saturation oxygen coverage (Θ_O^{sat} = 1.2 × 10^{15} atoms per cm^2) that can be achieved on the NP at $\Delta\phi$ = 1.38 V. Fig. 2 indicates that at very low potentials ($\leq \sim 0.65$ V), where no oxygen adsorbs on Pt surfaces, the most close-packed Pt(111) face is preferred and thus the NP shape is mainly enclosed by these faces (Fig. 2(a)). There are also small contributions from the (100) and (110) faces, which are the second and third stable surfaces.

Fig. 2(b) and (c) show that the equilibrium shape does not change much in the low to medium potential range of 0.7 V $\leq \Delta\phi < \sim 1.05$ V, where the O coverage ranges between 0.2 ML $\leq \Theta_O \leq$ 0.5 ML. This is because the relative stabilities change only slightly in this range. However, the ratios $\gamma_{520}/\gamma_{111}$, $\gamma_{730}/\gamma_{111}$ and $\gamma_{100}/\gamma_{111}$ decrease with $\Delta\phi$ (or Θ_O) for $\Delta\phi > \sim 1.05$ V ($\Theta_O >$ 0.5 ML). The surface free energy of (520) finally becomes smaller than (111) above ~1.24 V (1 ML) and thus (520) completely dominates the surface of NPs to form the THH shape that has been observed using TEM (Fig. 2(d)). Above 1.3 V (1 ML), the (100) surface is also more stable than (111). The difference between γ_{520} and γ_{100} is only ~4 meV $Å^{-2}$, which is certainly within the range of errors arising from technical and computational approximations. The coexistence of (520) and (100) faces results in the formation of Pt NPs with a truncated THH shape (Fig. 2(e)), which is very similar to the irregular THH shape observed in TEM images in Fig. 1(b).

Although, according to our calculations, PtO_2 bulk oxide becomes thermodynamically stable above ~1.04 V, there is no experimental evidence for formation of PtO_2 NPs. For instance, modeling the obtained TEM image was only possible with non-oxide surfaces. Therefore, THH Pt NPs represent metastable phases possibly stabilized as a result of kinetic limitations in the formation of PtO_2.

Fig. 3 shows the top views of clean and O-covered high-index Pt(520) and (730) surfaces at low, medium and high potentials. The (520) surface periodically consists of one (210) microfacet followed by one (310) microfacet, while (730) consists of two (210) microfacets followed by one (310) microfacet. Both surfaces have multiple-height stepped structures.

At a low potential of 0.70 V, O prefers to bind at four-fold hollow sites on the (210) microfacets of (520) and (730) surfaces and pulls together the adjacent Pt atoms. This phenomenon (known as row-pairing), leading to a packing of Pt surface atoms, has also been observed on low-index surfaces of other transition metals.[26–28]

The O-induced displacements of Pt atoms on high-index Pt(520) and (730) are expected to be larger than that on the close-packed surfaces. Consistent with that, upon increasing $\Delta\phi$ (Θ_O), a higher number of surface atoms relocate on (520)

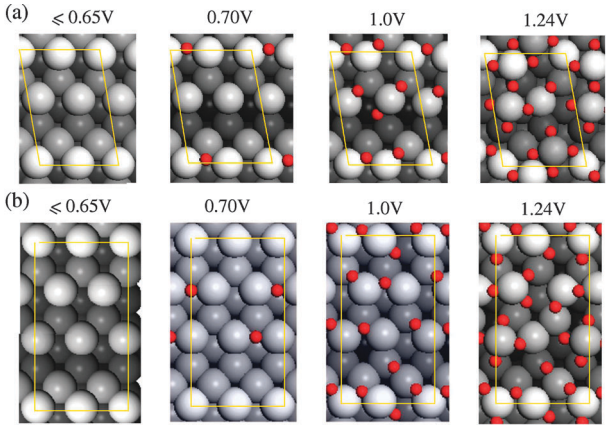

Fig. 3 Top views of the most stable structures of (a) Pt(520) and (b) (730) surfaces at different electrode potentials. The yellow lines indicate the surface unit cells that have been used in the calculations.

and (730) such that an optimum bond orientation and thus maximum bond strength can be achieved. At 1.24 V (1 ML), due to the O-induced packing of Pt surface atoms at the topmost layers (see Fig. 3), the (730) surface becomes as stable as the low-index (111) surface (see Fig. 2). The displacements of Pt atoms are much more drastic on (520) and can be viewed as a surface reconstruction. On this surface, O adatoms form a square overlayer to reduce the O–O repulsions and the Pt atoms of the third atomic layer move outward to form oxide-like PtO_2 structure together with the first atomic layer atoms.

We find that removing O adatoms from the reconstructed (520) surface causes this surface to become unstable, relaxing back to unreconstructed (520). Thus, from the thermodynamic viewpoint the polyhedron-shape should form upon decreasing the potential below 0.65 V (see Fig. 2(a)). However, experimental observations evidence that lowering the potential does not affect the shape of the THH NPs. The metastability of these roughened NPs at low potential is certainly due to the low mobility of the surface Pt atoms after removal of the O adatoms. This is to be contrasted with Pt atoms of the O-covered surface at high potential at which they become nearly oxidized. As a consequence, the barrier for surface atom mobility is lowered due to the electrochemical annealing[29] by O atoms, which explains the surface roughening observed under these conditions.

The contributions of different edges and corners of the particles to the overall surface free energy, which is the thermodynamic driving-force that leads to the formation of THH Pt NPs, are rather small. We expect that atom diffusion and reorganization barriers as well as O binding energy are slightly lower at these lower-coordinated sites, that might result in oxide formation at potentials even lower than 1.24 V and thus to earlier roughening of Pt nanoparticles.

In summary, we have shown that the atomically-rough Pt NPs consisting of high-index (520) faces can be synthesized in an aqueous electrolyte at high electrode potentials. O-induced formation of atomically-rough (520) faces leads to high (electro-)catalytic activity of the THH Pt NPs. Furthermore, we could show that by combining DFT calculations and thermodynamic considerations we are able to provide important quantitative information and physical insight into the morphological changes of the NPs with electrode potential under electrochemical conditions. Our study suggests that new interesting shapes of metallic NPs with high (electro-)catalytic activity can indeed be synthesized by tuning the electrolyte composition and electrode potential in electrochemical systems.

Acknowledgements

T.Z. thanks the Chinese Scholarship Council for financial support of a co-tutelle PhD study in The Netherlands. The Xiamen University authors thank the financial support of NSFC (grant no. 21021002). E.H. and R.A.v.S. acknowledge the National Computing Facilities (NCF) for providing computational resources (Grant: SH-170-11) and the National Research School Combination Catalysis for financial support. P. K. and T. J. acknowledge support from the the Bundesministerium für Bildung und Forschung (BMBF), the Deutsche Forschungsgemeinschaft (DFG) and the European Union (ERC-Starting Grant: THEOFUN).

References

1 R. A. van Santen, M. Neurock and S. G. Shetty, *Chem. Rev.*, 2010, **110**, 2005.
2 N. Lopez, T. V. W. Janssens, B. S. Clausen, Y. Xu, M. Mavrikakis, T. Bligaard and J. K. Nrskov, *J. Catal.*, 2004, **223**, 232.
3 A. Ueda and M. Haruta, *Gold Bull.*, 1999, **32**, 3.
4 N. Tian, Z. Y. Zhou and S. G. Sun, *J. Phys. Chem. C*, 2008, **112**, 19801.
5 F. Zaera, *Appl. Catal., A*, 2002, **229**, 75.
6 D. Astruc, F. Lu and J. R. Aranzaes, *Angew. Chem., Int. Ed.*, 2005, **44**, 7852.
7 R. M. Heck and R. J. Farrauto, *Appl. Catal., A*, 2001, **221**, 443.
8 N. Tian, Z.-Y. Zhou, S.-G. Sun, Y. Ding and Z. L. Wang, *Science*, 2007, **316**(5825), 732.
9 N. Hoshi, S. Kawatani, M. Kudo and Y. Hori, *J. Electroanal. Chem.*, 1999, **467**, 67.
10 S. G. Sun and J. Clavilier, *Chem. J. Chin. Univ.*, 1990, **11**, 998.
11 W. F. Banholzer and R. I. Masel, *J. Catal.*, 1984, **85**, 127.
12 G. Wulff, *Z. Kristallogr.*, 1901, **34**, 449.
13 E. Kaxiras, Y. Bar-Yam, J. D. Joannopoulos and K. C. Pandey, *Ab initio* theory of polar semicondutor surfaces. 1. Methodology and the (2 × 2) reconstructions of GaAs(111), *Phys. Rev. B: Condens. Matter Mater. Phys.*, 1987, **35**, 9625–9635.
14 M. Scheffler, *Physics of Solid Surfaces*, Elsevier, Amsterdam, 1987.
15 G.-X. Qian, R. M. Martin and D. J. Chadi, 1st-principles study of the atomic reconstructions and energies of Ga-stabilized and As-stabilized GaAs(100) surfaces, *Phys. Rev. B: Condens. Matter Mater. Phys.*, 1988, **38**, 7649–7663.
16 K. Reuter and M. Scheffler, Composition, structure, and stability of RuO_2(110) as a function of oxygen pressure, *Phys. Rev. B: Condens. Matter Mater. Phys.*, 2002, **65**, 035406.

17 F. Mittendorfer, N. Seriani, O. Dubay and G. Kresse, *Phys. Rev. B: Condens. Matter Mater. Phys.*, 2007, **76**, 233413.
18 T. Jacob, *J. Electroanal. Chem.*, 2007, **607**, 158.
19 P. Kaghazchi, K. A. Soliman, F. C. Simeone, L. A. Kibler and T. Jacob, *Faraday Discuss.*, 2008, **140**, 69.
20 P. W. Atkins, *Phys. Chem.*, Wiley-VCH, Weinheim, 1990.
21 V. Komanicky, H. Iddir, K. C. Chang, A. Menzel, G. Karapetrov, D. C. Hennessy, P. Zapol and H. You, *Electrochim. Acta*, 2010, **55**, 7934.
22 T. E. Madey, W. Chen, H. Wang, P. Kaghazchi and T. Jacob, *Chem. Soc. Rev.*, 2008, **37**, 2310.
23 J. A. Keith and T. Jacob, *ChemPhysChem*, 2010, **11**, 2779.
24 J. E. Mueller, J. Bandlow, P. Kaghazchi, and T. Jacob, in preparation.
25 DFT calculations were performed using the VASP code (Vienna *ab initio* Simulation Package)[30] using the PW91-GGA exchange–correlation functional.[31] The projected-augmented wave (PAW) method[32] was used to describe electron–ion interactions, and for valence electrons a plane wave basis set was employed. We established calculational parameters with an energy cut-off of 500 eV for all surfaces. The Brillouin zones of the (3×3)-surface unit cells of Pt(111), (100), (110) and (210) were sampled with (9×9), (5×5), (5×5) and (5×5) Monkhorst–Pack *k*-point meshes, respectively, while (2×2)-surface unit cells of both Pt(520) and (730) with (3×3) k-point meshes. The low-index surfaces (Pt(111), Pt(100), Pt(110)) were represented by 8-layer slabs, while the high-index Pt(210), (520) and (730) were represented by 10-layer, 12-layer and 15-layer slabs, respectively. The bottom 4 layers of the low-index surfaces, and 5, 6 and 6 layers of the high-index surfaces were fixed at the calculated bulk structure, and the geometry of the remaining layers was fully optimized (<0.001 eV Å^{-1}). In order to avoid interactions between period images, slabs were separated by a vacuum of at least 12 Å.
26 P. Kaghazchi, W. Chen, H. Wang, I. Ermanoski, T. E. Madey and T. Jacob, *ACS Nano*, 2008, **2**, 1280.
27 P. Kaghazchi and T. Jacob, *Phys. Rev. B: Condens. Matter Mater. Phys.*, 2007, **76**, 245425.
28 P. Kaghazchi and T. Jacob, *Phys. Rev. B: Condens. Matter Mater. Phys.*, 2010, **81**, 075431.
29 D. M. Kolb, *Prog. Surf. Sci.*, 1996, **51**, 109.
30 (*a*) G. Kresse and J. Hafner, *Phys. Rev. B: Condens. Matter Mater. Phys.*, 1993, **47**, 558; (*b*) G. Kresse and J. Hafner, *Phys. Rev. B: Condens. Matter Mater. Phys.*, 1994, **49**, 14251; (*c*) G. Kresse and J. Furthmuller, *Comput. Mater. Sci.*, 1996, **6**, 15.
31 J. P. Perdew, J. A. Chevary, S. H. Vosko, K. A. Jackson, M. R. Pederson, D. J. Singh and C. Fiolhais, *Phys. Rev. B: Condens. Matter Mater. Phys.*, 1992, **46**, 6671.
32 (*a*) P. E. Blöchl, *Phys. Rev. B: Condens. Matter Mater. Phys.*, 1994, **50**, 17953; (*b*) G. Kresse and J. Joubert, *Phys. Rev. B: Condens. Matter Mater. Phys.*, 1999, **59**, 1758.

